Civil and Environmental Engineering
Vol. 0, Issue 0, DOI: 10.2478/cee-2026-0067

Experimental Investigation of Wall Thickness Effect on Cold Joints in a Scaled Diaphragm Wall Model Using Fiber-Reinforced Self-Compacting Concrete

Rana F. YOUSEF [1, *], Haitham H. MUTEB [1], Ahmed AL-JANABI [1]

[1] Civil Engineering Department, University of Babylon, Babylon, Iraq.

* corresponding author: Eng.rana.falah@uobabylon.edu.iq

Date of Submission: 21 October 2025
Revision Date: 22 November 2025
Date of Acceptance: 23 November 2025

Civil and Environmental Engineering
Journal of the Faculty of Civil Engineering | University of Žilina

Abstract

Concrete diaphragm walls are crucial structural components for permanent retaining systems and deep excavation support. The research examines how wall thickness and cold joints influence the deformation behavior of diaphragm walls. A small laboratory model with a rigidity that is comparable to the field model was used for this purpose. The scaled model was designed to preserve the relative stiffness of the field model; however, due to the slenderness of the specimens, conventional reinforcement could not be applied. Instead, polypropylene fibers were used as an effective alternative to enhance crack resistance and ensure structural integrity. Four-point bending tests were carried out under static loading conditions using a laboratory compression testing machine. The model sizes are (40, 60, 80, and 100 mm) in prismatic thickness and overall width and length (900 mm and 2600 mm), respectively. Additional tests on 60 mm walls with one and two cold joints, and on 100 mm walls with two cold joints, were compared against joint-free specimens to assess the influence of cold joints. The findings indicate that increasing wall thickness improves load-bearing capacity and reduces lateral deformation. For proposed specimens maximizing strength gains when aspect ratio $(\frac{thickness}{depth})$ increase form $\frac{1}{40}\, to\, \frac{1}{30}$ and for increasing from $\frac{1}{60}\, to\, \frac{1}{40}$ deflection decreases sharply. Specimens with aspect ratio of $\frac{1}{40}$ one and two joints reduced ultimate load by about 3% and 15%, respectively, while at $\frac{1}{24}$ two joints caused a 10% reduction. Thinner walls proved more flexible and thus more sensitive to joint-induced weaknesses.

Keywords

small-scale deep excavation, diaphragm walls, Lateral displacement, cold joints, stiffness of diaphragm walls

1. Introduction

Deep excavation is an essential phase in the development of underground space in urban areas and diaphragm walls, which are configured by separate wall panels and vertical joints between panels, are widely used to brace excavations owing to the high rigidity, good integrity, and impermeability of the walls themselves (Comodromos et al., 2013; Houhou et al., 2019; Spruit et al., 2014, 2017). Over the past 60 years, diaphragm walls have become essential in deep excavations and groundwater control. Advances like thixotropic slurry, steel walls (1992), and soil-cement steel walls improved stability, strength, and efficiency. seismic active earth pressure tends to rise significantly toward the bottom of the wall (Mhawish &

Risan, 2024). Key success factors include proper joint sealing and panel overlap. Technologies such as hydro mills enabled deeper, more precise construction, while prefabricated systems offered speed but required larger excavations and higher costs. Continuous innovations are driven by practical experience and engineering progress. Lim et al. (2018) showed that thicker walls improve stiffness and reduce deformation, though gains diminish beyond certain limits. Similarly, Bleyhl (2018) emphasized optimizing thickness to balance efficiency and structural needs. Diaphragm walls are reinforced concrete barriers used as retaining and foundation walls in deep excavations. They provide stability against earth and water pressure, with fewer joints for better strength and water tightness. Capable of great depths and adaptable designs, they are especially suited for urban projects, making them a strong, versatile, and efficient solution in modern civil engineering (Liu et al., 2025; Wang et al., 2024). Panel joint modelling research underscores that ignoring real-world joint effects leads to underestimation of displacements and overestimation of bending moments. Cold joints between panels reduce stiffness and change deformation paths, especially in thicker diaphragm wall projects. Unlike conventional models that ignore joints, the proposed approach showed better agreement with field monitoring, excavation length, depth, and wall thickness influence the impact of joints, with greater effects in shorter and deeper excavations(Yang et al., 2024).

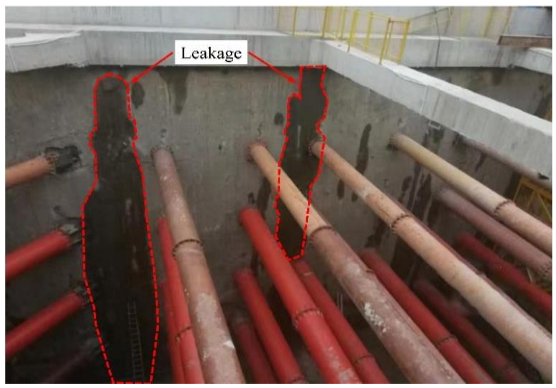

Figure 1: Leakage occurred at the joints between panels (Yang et al., 2024)

Moreover, thicker walls impose greater bending moments, increasing the importance of joint detailing and continuity where cold joints occur. This interplay highlights the need for accurate modelling workflows that incorporate both thickness and joint location effects.

Numerical modelling using the three-parameter Kerr foundation model shows that diaphragm wall thickness significantly controls both horizontal displacement and surface settlement during excavation. As thickness increases from 0.6 m to 1.4 m, horizontal displacement decreases by up to 28% and settlement outside the pit declines by 30% but raises bending moments. Designers must balance stiffness benefits against increased material costs and internal stresses (Li et al., 2024). Studies on rigid joints in diaphragm walls highlight the need for robust designs to mitigate degradation, stressing the negative impact of cold joints but overlooking their interaction with wall thickness a key focus of this research (Wang et al., 2024). Cold joints with as cast surfaces showed 31% higher shear capacity than those with plates (smooth surfaces) (Yousef et al., 2023).

Self-compacting concrete (SCC) is a special mix that flows easily into formwork and around steel without the need for vibration. It was created to save time, reduce labour, and improve quality, especially in tight construction areas. SCC, made with cement, water, aggregates, and superplasticizers, provides excellent workability, fewer voids, and better resistance to segregation and bleeding. When polypropylene fibres are added, the concrete becomes stronger, more flexible, and more resistant to cracking, bending, and impact, since the fibres help hold small cracks together and slow their growth (de Alencar Monteiro et al., 2018; Deng et al., 2023). Fiber-reinforced concrete (FRC) helps control shrinkage cracks, improves durability against corrosion and freeze-thaw cycles, and is especially effective near cold joints. Polypropylene fibres in high-strength concrete (M30 & M40) increase strength and reduce shrinkage and moisture loss, but lower workability. The optimum fibre content is 0.5%. Higher fibre length and dosage further delay cracking but reduce flowability (Mohod, 2015; Pereira et al., 2023; Roesler, 2019).

Adding fibers makes concrete more isotropic and ductile. Fiber-reinforced concrete shows higher compressive, tensile, and flexural strength, along with lower water absorption than normal concrete. Absorption increases over time in both types but eventually levels off. Reddy & Reddy (2023) Increasing fiber content reduced workability and compressive strength. At 0.2% fiber, the mix failed SCC standards, with 20% lower strength and 23% higher porosity. However, higher fiber content improved thermal insulation by reducing thermal conductivity (Barka et al., 2024). The plastic behaviour of the concrete employed in the diaphragm wall plays a critical role in maintaining the overall structural consistency (Ouedraogo et al., 2025).

This study introduces a novel experimental approach to examining the effect of diaphragm wall's thickness and cold joints by using a scaled laboratory model. Because replicating a diaphragm wall with realistic soil structure interaction is technically challenging, the wall was modelled and tested as a one-way slab to capture the essential structural response under lateral loading. This simplified but mechanically representative setup enables controlled investigation of parameters that are effect in real construction, providing new insight into their influence on diaphragm wall behaviour.

In the case of diaphragm wall construction, and because these walls are built in stages, the cold joint is parallel to the major moment M_x. At first glance, it appears that the location of the joint has no effect on its construction behaviour, but due to the biaxial state of stress (Timoshenko Plate Theory), it is expected that some stresses will exit in the transverse direction produced by the secondary moment ($M_y = -\upsilon M_x$).

2. Experimental Program

2.1. Specimen Design and Preparation

The experimental program consists of casting and testing four specimens monolithic with (40,60,80,100) mm thickness, two specimens 60mm thick with one and two cold joints. Last specimen is 100 mm thick with two cold joints. Plywood molds measuring 2600 × 900 × 100 mm were fabricated for each batch of specimens and cast outside the laboratory. Before each use, the molds were oiled and placed on level ground. Reinforcement consisted of six longitudinal deformed bars (Ø6 mm) with stirrups placed at 150 mm spacing and 15 mm cover. Plastic spacers were used to maintain the required clearances. All specimens were cast using Self-Compacting Polypropylene Fiber-Reinforced Concrete (SCPPFRC). Figure 2 illustrates the reinforcement layout and specimen preparation.

For specimens containing cold joints, 5 mm wooden separators were fixed inside the mold to divide the segments. After the first segment was cast and cured for seven days, the separator was removed to expose the joint surface. The subsequent segment was then cast following the same procedure: cleaning, oiling, placing reinforcement, and pouring fresh concrete against the hardened part. After 24 hours, the molds were removed, and the specimens were wrapped in wet burlap, which was moistened daily until 28 days of curing. Prior to testing, the specimens were cleaned and painted white to facilitate crack observation. All tests were conducted in the Structural Laboratory of the College of Engineering, University of Babylon. Figure 2 shows the layout and cross sections of these specimens; Table 1 lists the details of specimens.

Table 1: details of specimens

specimen	Wall thickness [mm]	Number of cold joints	aspect ratio $\frac{thickness}{depth}$
T40-0	40	0	$^1/_{60}$
T60-0	60	0	$^1/_{40}$
T80-0	80	0	$^1/_{30}$
T100-0	100	0	$^1/_{24}$
T60-1	60	1	$^1/_{40}$
T60-2	60	2	$^1/_{40}$
T100-2	100	2	$^1/_{24}$

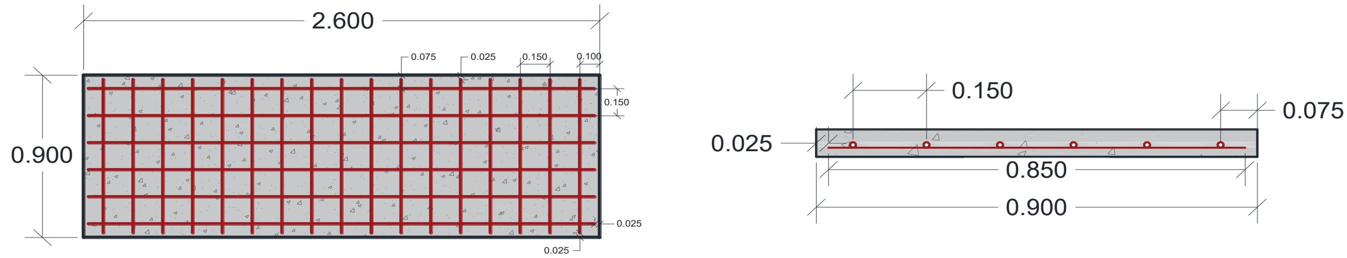

(a) Specimens without cold joints

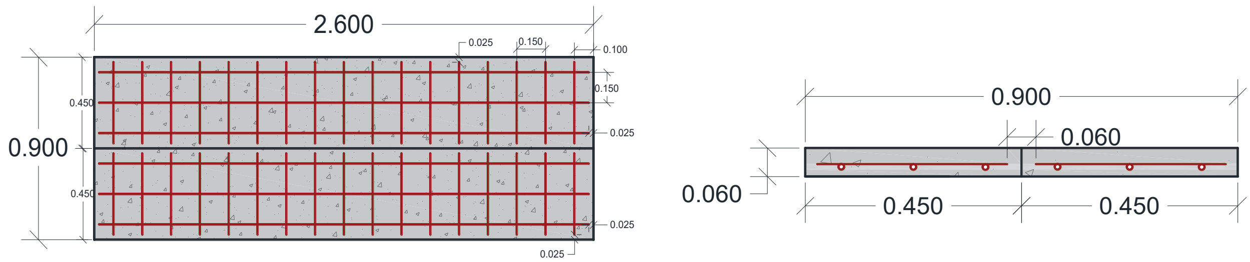

(b) Specimens with one cold joint

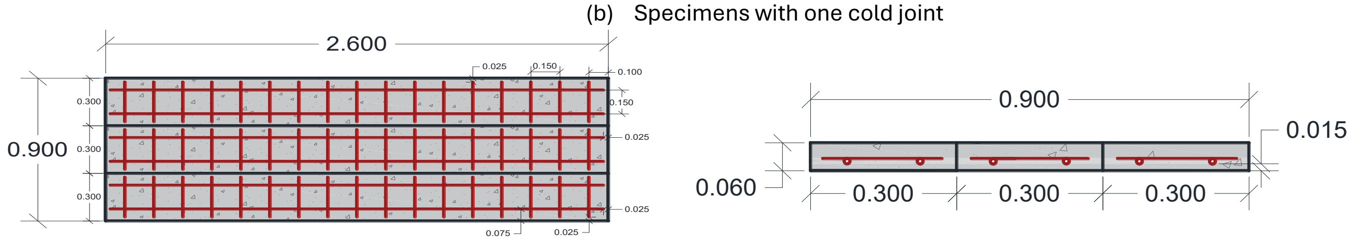

(c) Specimens with two cold joints

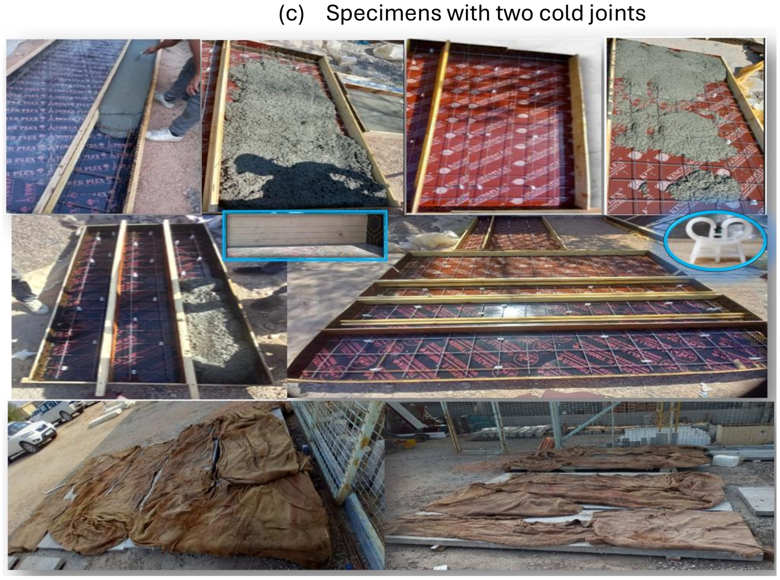

Figure 2: Specimens details (unite in m)

2.2. Materials

All materials used to prepare specimen's mixed were locally available. Ordinary Portland cement from (mass) factory conforming to Iraqi standard specifications (Iraqi Specification No.5, 2019). Al-Ekhaider sand was used as a fine aggregate (FA) in the substrate concrete mixes with a maximum size of particles 5 mm. Cursed and washed gravel from the Al-Nabai'i area with a maximum size of 10 mm was used and it conformed to Iraqi standard specifications (Iraqi specification requirements IQ.S 45, 2016). High execution short (12 mm), 910 $[kg/m^3]$ Density, 0.91Specific Gravity and white polypropylene fiber was used in this investigation that is manufactured by the SIKA company and fibrillated in pre-dosed pulp bags see Figure3. Mixing water used for all the mixes was normal tap water from the domestic water supply. So, it was clear of residual and organic materials that could have impacted on the concrete properties. The mix consists of Fly Ash as a filler to enhance the flowability and durability, reduce the amount of cement and heat of hydration, and super plasticizer (SP) commercially known as Sika's ViscoCrete 180 (Sika's ViscoCrete 180G, 2022) to increase segregation resistance and lower yield stress of concrete's mix. Deformed mild steel with an average diameter of 6 mm was used for reinforcement of specimens in this work satisfies ASTM A615 requirements (A 615/A 615M - 15a, 2015).

Figure 3: Polypropylene Fiber

Table 2: Mix proportions of Self-Compact Polypropylene Fiber-Reinforced Concrete (SCPPFRC)

Cement $[kg/m^3]$	**Fly Ash** $[kg/m^3]$	**Sand** $[kg/m^3]$	**Gravel** $[kg/m^3]$	**Water** $[kg/m^3]$	**Admixture S.P.** $[kg/m^3]$	**Polypropylene Fiber P.P.F.** $[kg/m^3]$
350	60^a	800	725	165^b	7^c	4.55^d
[a] Fly Ash=17% of cement weight, [b] w/b =40%, [c] S.P./b=1.7%and [d] Polypropylene Fiber =0.5% of total volume						
Mix strength grade, MPa at 28 days				38.71		

2.3. Mixing

The concrete mixing for SSC was achieved using a titling in a 0.1 m^3 horizontal rotary mixer machine. The procedure of SCC mixing was as follows: firstly, the fine and coarse aggregate, cement and Fly ash were mixed for two minutes then polypropylene fibres were added to the pan with mixing before adding half of the mixing water. Then Super plasticizer and remaining mixing water added to the constituents in the mixer. Mixing continued for two minutes to achieve uniform.

2.4. Fresh Self - Compacting Concrete Tests

To verify from being the concrete of the mixes is SCC, the four standard tests (Slump flow test, T50 cm slump flow test, V-funnel test, and L-box fresh test) of SCC were carried out on each batch, and the results were compared with the standard limitations mentioned in EFNARC (EFNARC, 2005). Table 3 shows the results of these tests. It can be noted that the results of these tests satisfy the requirements of EFNARC (EFNARC, 2005). Figure 4 shows the photographs of these tests.

Figure 4: V-funnel, slump flow and L-box tests of fresh concrete

Table 3: Fresh properties result of SCC mix

Mix	Properties related to self-compact ability			
	Slump flow [mm]	T50cm flow time [Sec]	V-funnel time [Sec]	L-box (H2/H1)
SCC^a	680	4	8	0.98
$SCPFRC^b$	615	6	21	0.76
Typical range of values (EFNARC, 2005)	650-800	2-5	6-12	0.8-1.0

a. SCC: Self - Compacting Concrete
b. SC-PFRC: Self-compact Polypropylene Fiber-Reinforced Concrete

2.5. Material Properties

For each batch of SCC, cube of (100 × 100 × 100 mm), cylinders of (200×100 mm), prisms of (100 × 100 × 400 mm) were cast with the beams to determine the mechanical properties of SCC. These specimens were cured under the same conditions as the corresponding structural members. Prior to loading the structural members, cube compressive strength (BS EN 12390-3, 2009). Cylinders Splitting tensile strength ASTM C496 (ASTM Standard C496, 2011) and flexural strength test prismatic body strength of the concrete were measured (ASTM C78/C78M-22, 2010), and the average values of twelve specimens were taken. The modulus of elasticity was determined according to (ASTM C469, 2011) the test was conducted using two cylindrical specimens measuring 150 × 300 mm. Mechanical properties of concrete shown in see Figure 5 and Table 4. The mechanical performance of three specimens of steel reinforcements was tested according to (A 615/A 615M - 15a, 2015). The properties of the reinforcing bars are presented in Table 5.

Figure 5: Shows the testing process of the concrete material parameters.

Table 4: Mechanical properties of concrete

Compressive Strength [MPa]	Splitting tensile strength [MPa]	Flexural strength [MPa]	Elastic Modulus [GPa]
38.71	4.86	4.62	33

Table 5: Mechanical properties of steel reinforcements

Nominal diameter [mm]	Actual Diameter [mm]	Yield Stress [MPa]	Ultimate Stress [MPa]	Elastic Modulus [GPa]
6	5.9	430	560	200

3. Test Setup and Measurement System

The experimental setup was designed to evaluate the flexural behavior of diaphragm wall specimens under varying conditions. All specimens were prepared with standardized dimensions and reinforcement details, enabling direct comparison of many thicknesses and the presence of cold joints. A four-point bending arrangement was adopted, using a centrally positioned hydraulic jack to apply the load, which was evenly distributed across the specimen through steel loading plates.

Deflections were continuously monitored with Linear Variable Differential Transformers (LVDTs), providing accurate measurements as the load was applied incrementally. Before commencing the formal loading, a trial load was applied to eliminate gaps between components and verify system integrity. The loading procedure followed established protocols, beginning in force control mode and transitioning to displacement control as the specimens approached their ultimate capacity. To test a simply supported one-way slab (2400 mm × 900 mm), the specimen was placed on a hydraulic testing machine with a 2400 mm clear span and 100 mm overhangs. Two-line loads were applied 800 mm apart at mid-span using a hydraulic system, simulating soil pressure on retaining walls. Steel plates (20 mm thick, 100 mm wide) and rubber pads (10 × 100 mm) were used at load and support points to distribute forces evenly and reduce stress concentrations. Unlike rigid loads, soil pressure remains perpendicular to the wall's surface during deformation, requiring accurate simulation of its direction-dependent behavior. Rigid loading elements limit realistic deflection patterns and stress distribution. Therefore, rotatable loading segments were used to better mimic soil pressure, capturing complex bending and moment effects.

A specially designed support system with three semicircular steel bearings ($\sigma y \geq 400$ MPa) was implemented, one fixed central bearing and two side bearings allowing transverse rotation. This setup replicates the nonlinear flexural behavior of retaining walls under lateral earth pressure by converting vertical loads into realistic bidirectional bending moments. All specimens were tested to failure using a calibrated electro-hydraulic testing machine (capacity: 2500 kN) at the Structural Laboratory, University of Babylon. The loading system included a rigid steel base anchored to a concrete foundation, with a central hydraulic jack and piston. A rigid steel portal frame comprising two vertical columns and a top lateral beam supported the setup. An adjustable-height box girder acted as a stopper for upward movement.

Loading was applied in load control mode at a constant rate of 0.5 kN/sec. Each specimen underwent a two-line loading test, with loads applied at one-third span points. Test setup and instrumentation details are shown in Figures 7. During the experiment, it was necessary to record the specimens' characteristic loads, specifically cracking, yielding, and ultimate load.

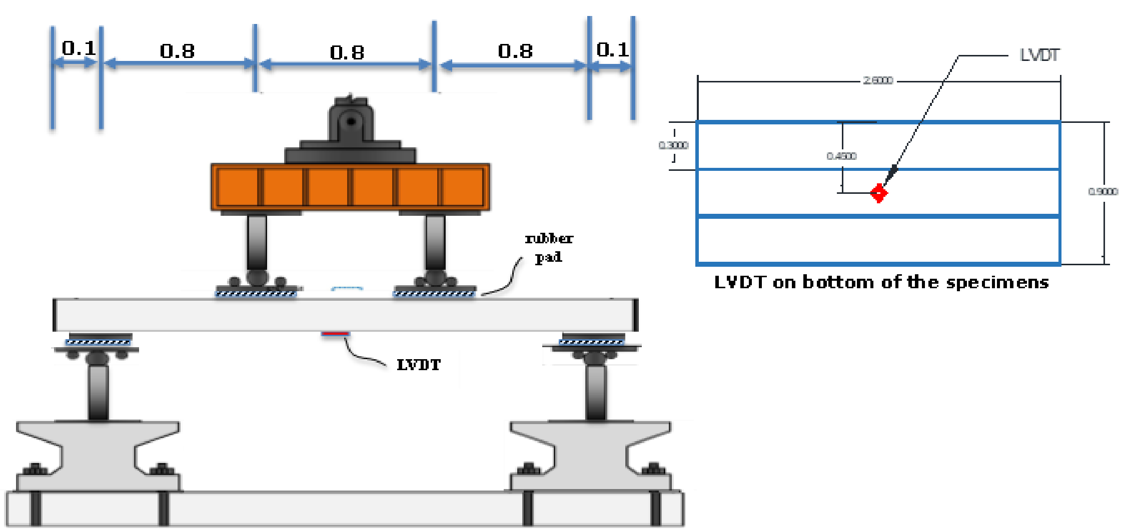

Figure 6: Schematic diagram of the specimen monitoring system (unit: m)

Figure 7: Experimental Loading Setup System

4. Results and Discussion

Diaphragm walls have been extensively evaluated for thicknesses of (40, 60, 80, and 100) mm, each offering distinct structural characteristics impacting performance underload as shown at Figure 8. A 40 mm wall bends more because it's less stiff, so it fits light-duty cases. A 60 mm wall balances strength and flexibility, good for tight urban sites.

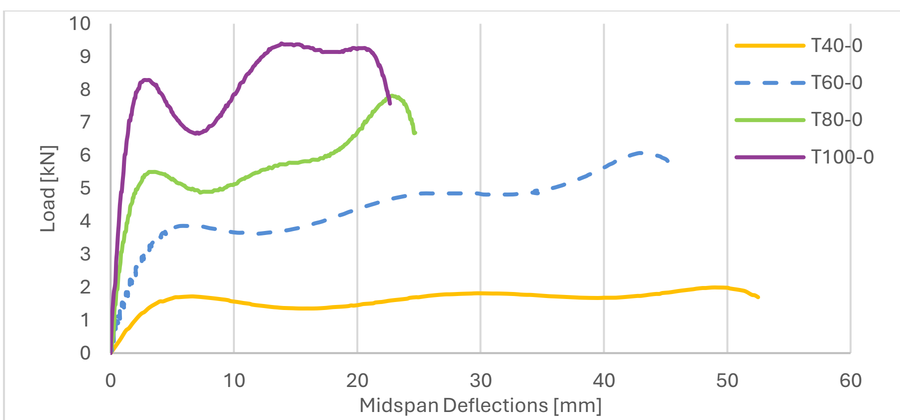

Figure 8: Load- midspan deflection curves of specimens with different thicknesses

At specimen with 80 mm, performance improves with higher stiffness and lower deflection, making it fit for deeper digs. The 100 mm wall gives maximum strength and minimal deformation, ideal for tough soil and high safety needs. Overall, evaluating these thick variations highlights best practices for diaphragm wall construction, providing insights into their appropriateness for various engineering applications based on specific performance requirements (Yang et al., 2024; Zhang et al., 2021). Yield deflection is the deflection at which the material begins to yield (plastic deformation begins). Thicker walls slightly reduce yield deflection, likely due to increased stiffness, but the effect is less pronounced compared to max deflection. To determine the yield load and yield displacement from load–deflection curve, usually follow Tangent Intersection Method by Extend the initial elastic slope line until it intersects with a line drawn through the plastic portion of the curve; the intersection is the yield point.

Table 6: Characteristic loads, midspan deflections of specimens with different thickness

specimen	Stiffness Ratio	P_{yield}	δ_{yield}	$P_{ultimate}$	$\delta_{ultimate}$	P_{cr}
	EI/γ_{w*h^4}	[kN]	[mm]	[kN]	[mm]	[kN]
T40-0	434	1.70	5. 60	2	49.25	1.72
T60-0	1465(↑238%)*	3.80(↑124%)*	5.40 (↓**4%**)*	6.07(↑**204%**)*	43.55(↓12%)*	3.86(↑124%)*
T80-0	3472(↑700%)*	5.40(↑218%)*	2.80 (↓**50%**)*	7.8(↑**290%**)*	22.80(↓54%)*	5.50(↑220%)*
T100-0	6782(↑1463%)*	8.20(↑382%)*	2.38(↓**58%**)*	9.40(↑**370%**)*	13.85(↓72%)*	8.28(↑381%)*

Note: P_{yield}, δ_{yield} *is the yield load and yield midspan deflections;* $P_{ultimate}$, $\delta_{ultimate}$ *is the ultimate load and ultimate midspan deflections;* P_{cr} is the cracking load noted from experimental testing.
* Compared with specimens with 40mm thickness.

Figure 9 shows that increasing wall thickness reduces both maximum and yield deflection, but the effect is much stronger on maximum deflection. From 40 to 80 mm, deflection drops sharply, especially between 60–80 mm, indicating a threshold where stiffness improves rapidly. Beyond 80 mm, further gains are small, making extra thickness less efficient. Yield deflection decreases only slightly with thickness, staying under 60 mm throughout. Overall, the results highlight 60–80 mm as the most effective range for performance improvement without unnecessary material use.

From 80 mm to 100 mm, the rate of improvement slows down. Beyond a certain point, adding more material provides less gain in deflection reduction, possibly making it economically inefficient. This data helps identify an optimal wall thickness where deflection performance improves significantly without unnecessary material use.

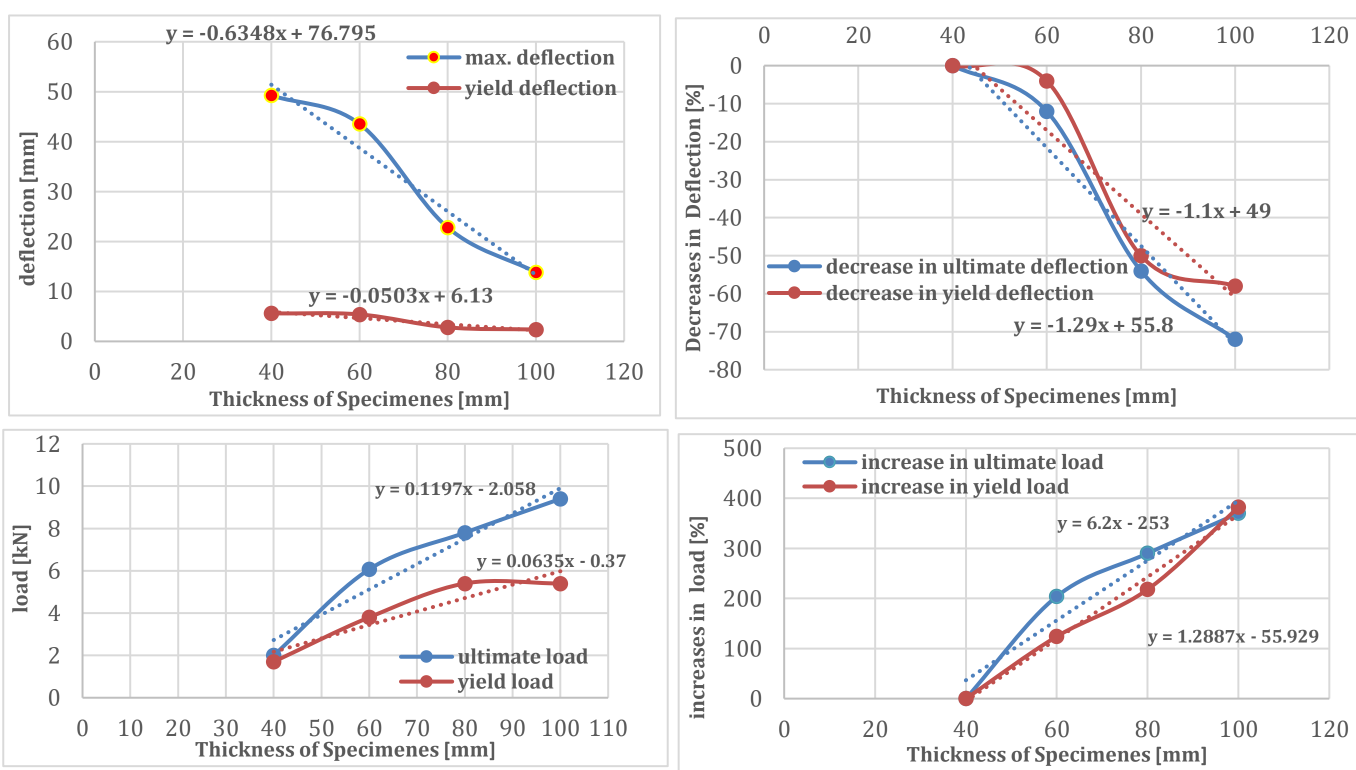

Figure 9: Relations of Load and Midspan deflection with different thicknesses of specimens

The results presented in Figure 8 show that the percentage increase in both yield load and ultimate load generally improves with increasing specimen thickness. A sharp improvement is observed as the thickness increases from 40 mm to 60 mm, which can be attributed to enhanced stiffness, better stress distribution, and higher resistance to cracking. Beyond 60 mm, the rate of improvement becomes less pronounced, and the curves begin to plateau, particularly for the ultimate load at around 70–80 mm, suggesting diminishing returns in strength enhancement with additional thickness. This behavior may be explained by reduced material efficiency at larger dimensions and the onset of other failure mechanisms such as shear or local crushing, which limit further gains in load capacity. Overall, the findings highlight that increasing thickness is most effective in the range of 40–60 mm, while beyond 80 mm the structural benefit is marginal. For efficient deflection control, the critical range lies between 60 mm and 80 mm thickness. Beyond that, alternative design strategies may be more cost-effective than further thickening.

5. Different Walls Cold Joints Evaluated

Cold joints form when there is a delay between consecutive concrete pours, creating a discontinuity and a weaker bond between layers. In diaphragm walls, such joints can adversely affect structural performance, particularly in terms of water tightness and shear capacity. Specimens containing cold joints exhibit reduced stiffness and bond deterioration, which in turn lower both yield and ultimate loads. The specimens with thicknesses of 60 mm and 100 mm were selected to study the behaviour of cold joints because they represent two distinct stages of structural response, 60 mm thickness represents the transition point where stiffness gains start to diminish, while 100 mm represents a highly stiff section where other factors govern behaviour. Comparing them highlights differences between the transition stage and the high-stiffness stage.

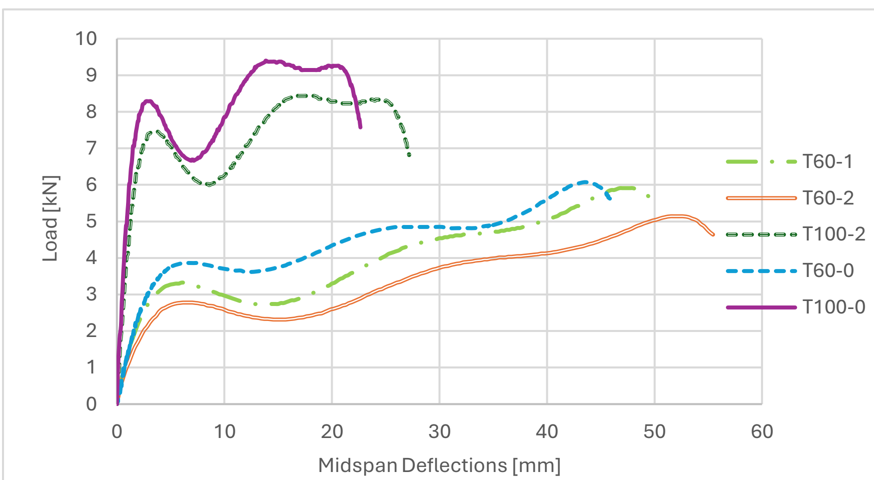

Figure 10: Load- midspan deflection curves of specimens with cold joints

The integrity of walls decreases as cold joints increase, see Figure 10. Creating weak planes and leakage risks. Thin walls (60 mm) are highly susceptible, while thicker walls (100 mm) show better but still limited resistance. Most of the wall movement happens at the joints, not within the panels themselves, which explains why cracks and leaks usually appear along these connections during excavation. To reduce this risk, continuous concrete pouring is best. If joints can't be avoided, they must be properly prepared and treated, with strict quality control and good planning to ensure the wall remains durable and structurally sound. Yousef et al. (2022) showed mechanical connectors, especially hooked reinforcing bars in UHPFC shear pockets have proven to be the most effective in enhancing the performance of cold joints in diaphragm walls, their practical application remains difficult due to construction complexity and site limitations. Grooved surfaces combined with UHPFC provide the strongest and most reliable bond with NC substrates, making this method effective for overlay applications and cold joint connection (Al-Rubaye et al., 2020).

Table 7: Characteristic loads, midspan deflections of specimens with cold joints

specimen	Stiffness Ratio	P_{yield}	δ_{yield}	$P_{ultimate}$	$\delta_{ultimate}$	P_{cr}
	EI/γ_{w*h^4}	[kN]	[mm]	[kN]	[mm]	[kN]
T60-1	1465	3.1(↓18%)*	5.0(↓7%)*	5.9(↓3%) *	48.00(↑10%)*	3.32(↓14%)*
T60-2	1465	2.65 (↓30%)*	4.9 (↓9%)*	5.14(↓15%)*	52.92 (↑22%)*	2.78(↓28%)*
T100-2	6782	7.4 (↓10%)*	3.0 (↑26%)*	8.46(↓10%)*	16.62(↑20%) *	7.46(↓10%)*

Note: $P_{yield}, \delta_{yield}$ *is the yield load and yield midspan deflections;* $P_{ultimate}, \delta_{ultimate}$ *is the ultimate load and ultimate midspan deflections;* P_{cr} is the cracking load, * Compared with specimen have same thickness but without cold joint.

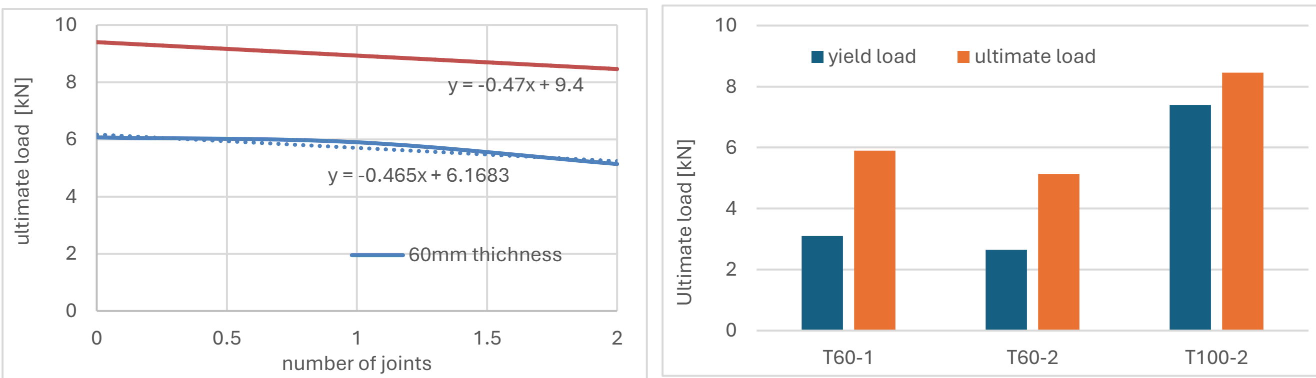

Figure 11: Effect Number of cold joints on load of specimens

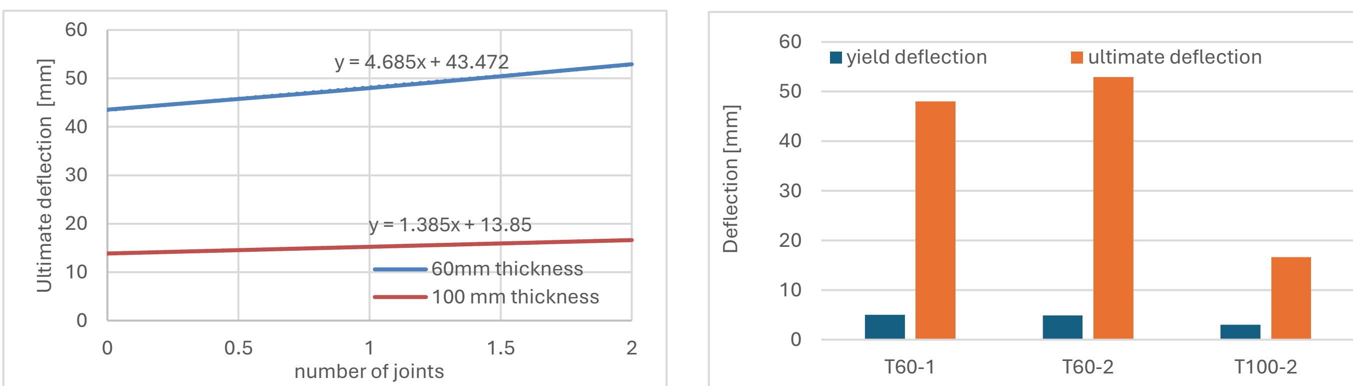

Figure 12: Effect Number of cold joints on midspan deflection of specimens

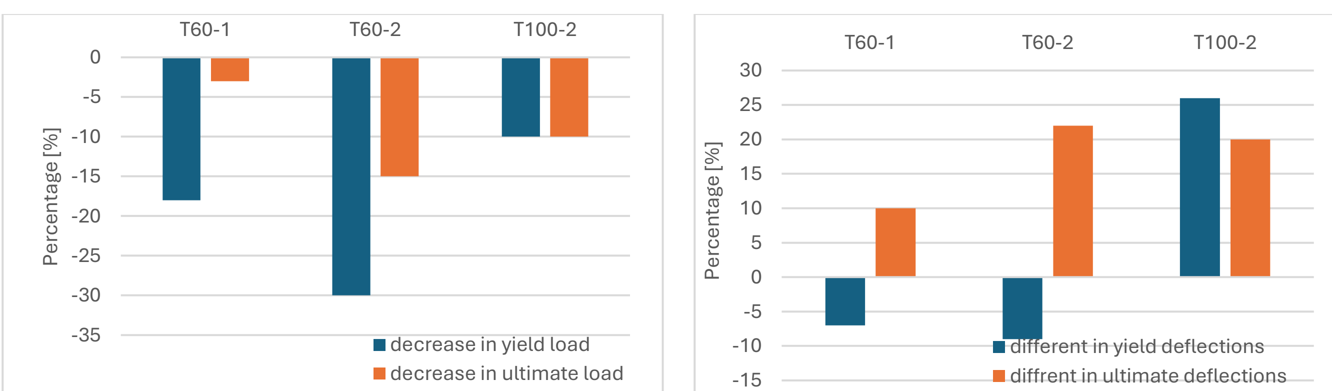

Figure 13: Effect Number of cold joints on variation of load and midspan deflection of specimens

The results in Figure 11 show that increasing the number of joints leads to a reduction in both yield and ultimate loads, accompanied by an increase in ultimate deflections, see Figure 12. Conversely, the thinner 60 mm walls are more flexible and therefore more sensitive to joint-induced weaknesses. Although both thicknesses showed a similar rate of reduction in ultimate load with additional joints (around 0.47 per joint), the 100 mm thick consistently sustained higher loads and experienced smaller deflection increases.

This effect is more pronounced in the 60 mm slabs, which exhibited greater losses in load capacity and larger growth in deflections compared to the 100 mm slabs. Overall, the findings highlight that while joints negatively impact structural performance, greater slab thickness improves load-bearing capacity and reduces sensitivity to jointing effects.

From Figure 12, it can be observed that deflection increases more rapidly with the number of joints for specimens with 60mm thickness with a larger slope (4.685). In contrast, specimens with a thickness of 100 mm show a smaller slope (1.385), suggesting that deflection develops more gradually as the number of joints increases. This behaviour can be attributed to the greater stiffness, strength, and stress redistribution capacity of the thicker walls which effectively limit deformation.

Figure 13 showing the deformation ratio indicates a reduction at the yielding stage in 60 mm specimens with one or two cold joints. However, performance comparisons in this study are based on ultimate deflection, as yielding is affected by early micro-cracking and local stiffness variations from the cold joints. Ultimate deflection better represents the overall structural behaviour, energy absorption, and post-yield capacity, providing a more reliable basis for comparison.

Yang et al. (2024) compares the maximum calculated displacements obtained by Proposed and Conventional approaches in PLAXIS, his results indicate that cold joints have a greater effect on thicker diaphragm walls, contrary to laboratory findings in this study. This discrepancy arises can be due to the numerical model without joints predicting unrealistically small deflections, making the difference between the two approaches appear larger for thicker walls. Alternatively, the discrepancy may be attributed to the joint-linking method in the PLAXIS program or to the segment length-to-thickness ratio adopted in the models.

Superczyńska et al. (2016) studied Numerical Analysis of Diaphragm Wall Model Executed in Poznań Clay Formation Applying Selected FEM Codes presented numerical analyses of a diaphragm wall model in the Poznań clay formation using two FEM codes, Plaxis and Abaqus. The constitutive clay models adopted in both platforms were evaluated against field measurements. The closest agreement with the observed horizontal displacement of 15.0 mm was achieved using the Abaqus Coulomb-Mohr model but Plaxis gave higher displacement. These findings underscore the necessity of exercising caution in geotechnical FEM applications, as the accuracy of results is strongly influenced by the chosen constitutive model, numerical integration algorithms, finite element types, and Gauss point configurations.

Failure Mode of Thinner walls (40-60 mm) exhibited distributed cracking patterns with gradual stiffness degradation, while thicker specimens (80-100 mm) failed through sudden crushing after limited plastic deformation, see Figure 14. The 60 mm specimens with cold joints showed unique hybrid failure modes initial joint separations at 70% of ultimate load, followed by distributed cracking until final collapse. This two-phase failure process explains their enhanced ductility, as joint openings accommodated additional deformation without immediate structural collapse (Qiu et al., 2023).

Figure 14: Failure Mode

6. Influence Dimensions of Segments on Maximum Diaphragm Wall Deformation

The wall depth of excavation -to-thickness ratio (H/T) and segment length-to-thickness ratio (L/T) significantly influence stability and construction efficiency. Figure 15 shows specimens with low L/T values (<5) show greater stiffness and better joint deformation control, supporting Kisan et al. (1996)(Kisan et al., 1996), who noted that shorter panels are stabler, especially in soft ground. In contrast, the specimens reported in Ming Yang's (2024)(Yang et al., 2024) study exhibit higher L/T ratios, which can increase the flexibility of the wall segments and cause excessive lateral deflections in thicker specimens influenced by joints.

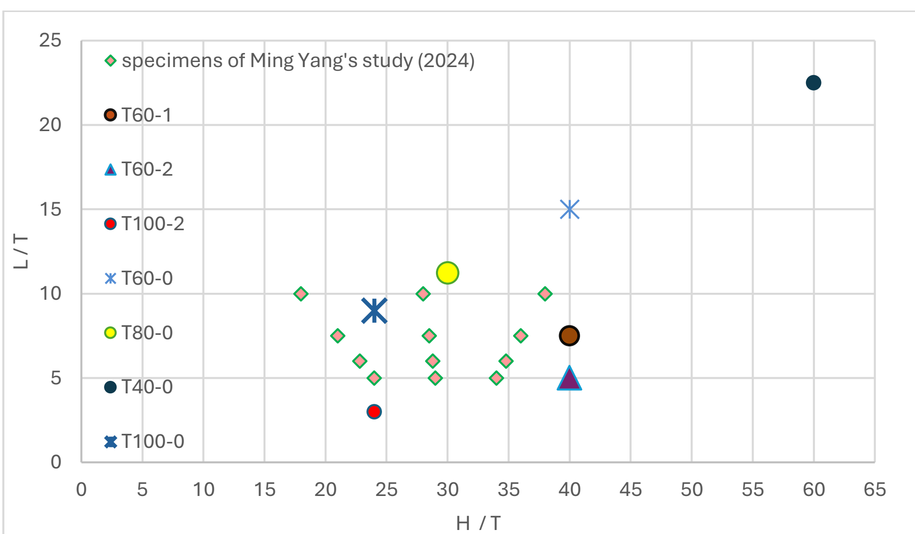

Figure 15: Relationship between length of the segments (L) to its thickness (T) and depth of excavation (H) relative to thickness (T)

In this study, experimental results demonstrated that specimens with ratio of panel's length to wall thickness is less than 5 and ratio of excavation depth to wall thickness is less than 25 exhibited 23-35% greater stiffness and superior joint deformation control compared to those with higher ratios. The structural response of the wall appears to be largely unaffected by the discontinuities introduced by cold joints. This observation is consistent with design recommendations indicating that walls with relatively low slenderness are less sensitive to construction imperfections or localized weaknesses.

Comparable findings have been reported in studies on diaphragm wall performance, such as those discussed by Gaba (Gaba et al., 2003), which emphasize the importance of wall thickness and geometric proportions in maintaining stability and limiting deflection. The ratio between segment length and thickness significantly impacts diaphragm wall load distribution. A high ratio causes slenderness, reducing stiffness and concentrating stresses at joints, leading to uneven load distribution. Lowering the ratio by increasing thickness or reducing length improves stiffness and ensures more uniform load transfer. Maintaining a moderate length-to-thickness ratio (less than 15:1) helps prevent stress concentrations and achieves balanced load distribution.

From Figure 16 a numerical fit of the data is Equation 1 that indicates maximum lateral displacement from length to thickness of segments.

$$\delta_{hmax} = 0.8852\frac{L}{T} + 26.021 \quad (1)$$

Where:
L - length of segments,
T – thickness of segments.

The segment's length-to-thickness ratio affects stress distribution, wall deformation, and soil pressure. A small ratio leads to uniform stress and smaller deformations, while a larger ratio increases localized pressure and lateral movement. However, its overall impact on maximum displacement is moderate, so it should be treated as a secondary factor compared to key design parameters like support stiffness, wall depth, and soil conditions. which aligns with similar conclusions in previous research(Yan et al., 2025).

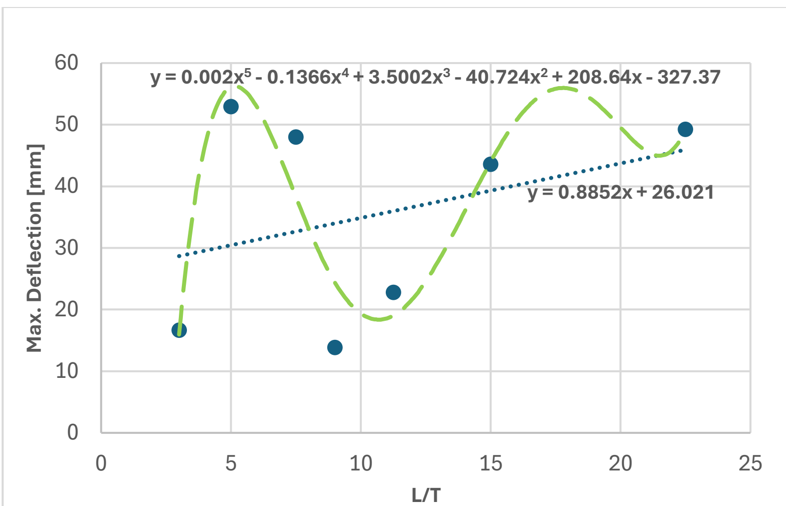

Figure 16: Relationship of segment length-to-thickness ratio and the maximum lateral displacement δ_{hmax} of the diaphragm wall

7. Wall system stiffness

Supporting system stiffness affects excavation performance (Addenbrooke, 1994; Potts, D. M., and Day, 1990). Clough, G. W., and O'Rourke (1990) explained wall system stiffness as Equation 2.

$$S = EI / \gamma_w h^4 \quad (2)$$

Where:
S - wall system stiffness,
E - Young's modulus assumes 30 GPa for concrete,
I - moment inertia of the wall,
h - vertical spaces of struts,
γ_w - vertical spaces of struts.

The equation represents a relative stiffness parameter of the wall (sometimes called Wall Stiffness Factor or Stiffness Ratio). It is a dimensionless parameter used to evaluate the stiffness of a wall relative to soil or water pressures. Figure 17 describes the data of maximum wall deflection to excavation depth ($^{\delta_{hmax}}/_{H_e}$)and the wall system stiffness against the factor of safety (FOS) against basal heave as defined by Mana, A. I. (1981).

Moormann's results Moormann (2004) agreed that maximum wall deflection normalized reduces just slightly with the increase of wall system stiffness and in a dispersed distribution. This indicates that a wall that is more adaptable (and hence more cost-effective) may be adequate in several situations. The global design approach for cantilever walls should be used carefully. A deficit of adequate bracing or support during excavation can lead to larger deformations in the clay, mirroring the behavior of softer soils under similar conditions. This analysis requires valuable insights into how different cities do excavation-induced lateral wall movements. It focuses on the importance of studying local conditions and design observations in predicting and adjusting these movements. The use of system stiffness as a predictor of movement appears to be a useful tool across various geological and urban contexts.

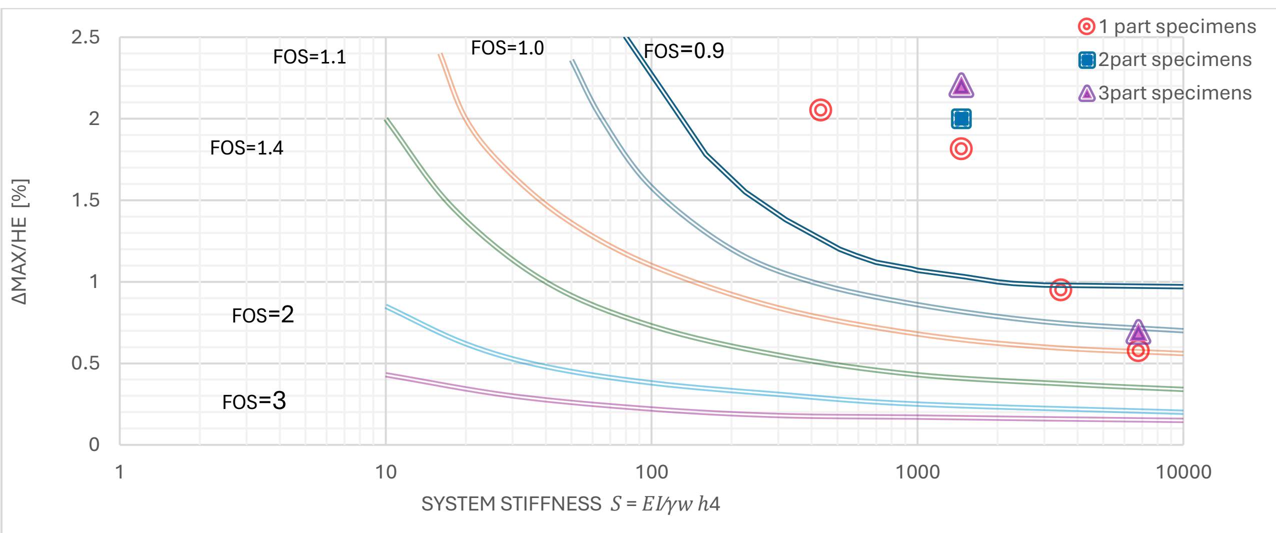

Figure 17: Relationship of Maximum Wall Deflection and Wall's System Stiffness (Mana & Clough, 1981)

The analysis demonstrates that the presence of cold joints significantly increases the lateral deflection of the wall, thereby reducing the factor of safety, even though the nominal structural stiffness of the system remains constant. This reduction in performance is particularly critical for thinner walls, where the relative influence of cold joints is more pronounced, rendering them more vulnerable to instability and serviceability concerns compared to thicker sections.

8. Ductility Index Results

Ductility is used to evaluate the ductility of reinforced concrete structures with expressions of deflection, curvature, or rotational ductility, and it is defined as the ability of a structural element to undergo inelastic deformations without significant loss in resistance (John Newman, 2003). The ductility has been calculated using displacement method for the reinforced concrete specimens, the ductility is expressed in terms of ductility index. The ductility index, μΔ was used to quantify the ductility performance of the specimens, it is the ratio of the mid-span deflection at ultimate or failure (Δu) to that deflection at the yielding point (Δy) that calculated from Tangent Intersection Method (Park & Paulay, 1991).The ductility indices for all tested specimens are given in Table 4.

Table 8: Ductility index of tested specimens

specimen	δ_{yield} [mm]	$\delta_{ultimate}$ [mm]	Ductility $\mu = \frac{\delta_{max}}{\delta_{yield}}$
T40-0	5. 60	49.25	8.80
T60-0	5.40	43.55	8.10
T80-0	2.80	22.80	8.00
T100-0	2.38	13.85	5.82
T60-1	5.00	48.00	9.00
T60-2	4.90	52.92	10.80
T100-2	3.00	16.62	5.50

Thinner walls (40–60 mm) exhibit higher ductility, meaning they can undergo larger deformations before failure, see **Figure 18**. In contrast, thicker walls (around 100 mm) are stiffer but less ductile, indicating a trade-off between stiffness and ductility and failures due to sudden crushing or brittle fractures after reaching a high yield stress.

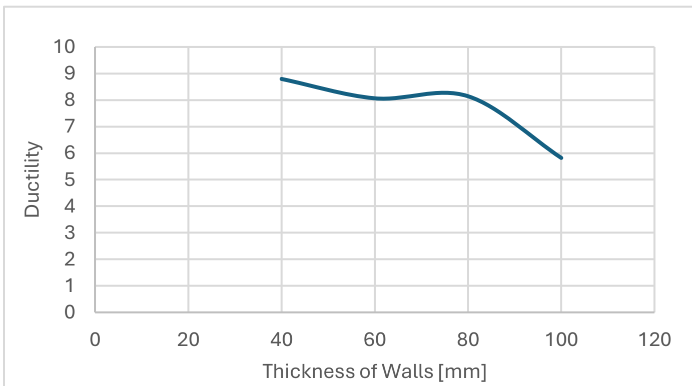

Figure 18: Ductility of specimens with different thicknesses

Contrary to expectations, cold joints improved ductility in 60 mm specimens, with two-joint configurations (T60-2) achieving a 33% higher ductility index (10.8) than joint-free walls (8.1), see Figure 19. This phenomenon stems from joint-induced stress redistribution, which delays localized failure and enables more uniform deformation across the specimen length. However, this benefit came at the cost of 15% reduced ultimate load capacity, highlighting a tradeoff between deformation capacity and strength. Thicker 100 mm walls showed no such ductility improvement, with cold joints reducing both load capacity (10%) and ductility (5%), indicating that joint effects become predominantly detrimental in stiffer sections.

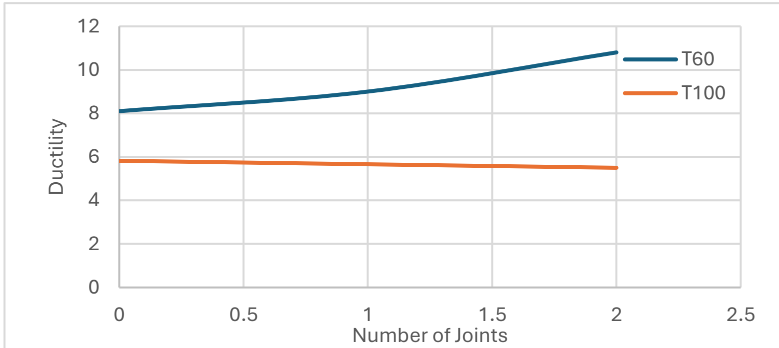

Figure 19: Ductility of specimens with number of cold joints

The farthest-point method can also be employed to determine the yielding load (Feng et al., 2017). As shown in Figure 20, a straight line is drawn from the origin of the midspan load–displacement curve to its peak. The yielding point is defined as the location on the curve that lies farthest at a perpendicular distance, from this line. For the processing of yield force and yield displacement, the simplified method for determining the yield point proposed by Peng Feng is applied (Feng et al., 2015).

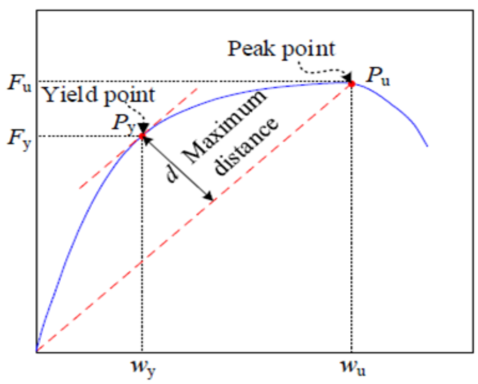

Figure 20: Definition of yielding load (Feng et al., 2017)

$$\max d = \frac{|P_u * w_y - w_u * P_y|}{\sqrt{{P_u}^2 + {w_u}^2}} \tag{3}$$

Where:
P_y - yielding point,
F_y - yielding load $0 < F_y < F_u$,
w_y - yielding deflection $0 < w_y < w_p$,
P_u - peak point,
F_u - peak load,
w_u - deflection at peak load,
d_{max} - maximum distance from the line.

Figure 21show maximum distance from the line (d_{max}), for more than one point met the criterion the yielding point was taken as the average of those points. The yielding load determined using the Farthest Point Method shows excellent agreement with that obtained from the Tangent Intersection Method, thereby demonstrating that both methods provide a reliable and efficient means for evaluating the yielding load.

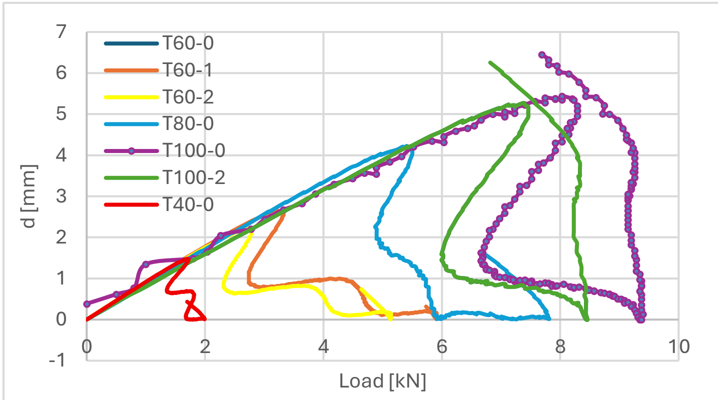

Figure 21: Relation the load with distance from the line

Table 9: Definition of yielding load by Farthest Point Method

specimen	Wall thickness	Number of cold joints	d_{max}	P_{yield}	δ_{yield}	P_{yield} by Tangent Intersection Method
	[mm]	------	[mm]	[kN]	[mm]	[kN]
T40-0	40	0	1.48	1.70	5.25	1.70
T60-0	60	0	3.03	3.78	5.22	3.80
T80-0	80	0	4.23	5.41	2.75	5.40
T100-0	100	0	5.44	8.03	2.30	8.20
T60-1	60	1	2.65	3.22	4.75	3.10
T60-2	60	2	2.22	2.72	5.04	2.65
T100-2	100	2	5.27	7.38	2.88	7.40

9. Conclusions

- The study shows that thickness of a Scaled Diaphragm Wall Model Using Fiber-Reinforced Self-Compacting Concrete has a major impact on load-bearing capacity and flexural performance. Tests reveal that increasing thickness from 40 mm to 100 mm (raises stiffness and moment capacity) significantly improves strength and reduces deflection, with the most effective range being 60mm to 80mm. Beyond this range, the wall becomes so stiff that material limitations control its behavior (not thickness), additional thickness only increases weight with very little structural benefit, indicating an optimal threshold for efficient design.

- Cold joints were found to degrade thinner walls, reducing ultimate load capacity by up to 15% in ultimate load capacity for 60 mm walls with two joints may seem modest, the accompanying 28% increase in deflection could have significant consequences for serviceability, particularly in water retaining structures where joint leakage is a critical concern. That is because their reduced cross-section makes them more sensitive to discontinuities in bonding and stiffness. While thicker walls can better redistribute stresses around cold joints, making them more resilient. These findings challenge conventional assumptions about linear performance gains with increasing thickness and highlight the importance of strategic joint management in staged construction.

- Specimens with L/T < 5 and H/T < 25 showed 23–35% higher stiffness and superior joint deformation control, confirming that walls with low slenderness are less sensitive to cold joints and construction imperfections. High L/T ratios, however, increase wall flexibility, stress concentrations, and lateral deflection.

- Experimental results indicate that while the segment's length-to-width ratio influences stress distribution and wall deformation that larger ratios increase localized pressures and lateral movement, its effect on maximum lateral displacement is moderate compared to other parameters such as support stiffness, wall depth, and soil conditions.

- larger ratios increasing localized pressures and lateral movement. However, its effect on maximum displacement is moderate, making it a secondary consideration relative to primary design factors such as support stiffness, wall depth, and soil conditions.

- The analysis shows a trade-off between stiffness and ductility in diaphragm walls: thinner walls (40–60 mm) offer higher ductility and can sustain larger deformations before failure, while thicker walls (100 mm) are stiffer but less ductile, making them more prone to sudden crushing or brittle fractures once high yield stress is reached.

- Cold joints unexpectedly enhanced ductility in 60 mm specimens, with two-joint walls achieving a 33% higher ductility index than joint-free walls, due to stress redistribution delaying localized failure. This improvement, however, reduced ultimate load capacity by 15%, showing a tradeoff between strength and deformation capacity. In contrast, 100 mm thick walls showed no ductility benefit, as cold joints instead reduced both load capacity (10%) and ductility (5%), suggesting that in stiffer sections, joint effects are mainly detrimental.

- The observed ductility improvements from cold joints in 60 mm specimens can be due to create transitional interface zones that allow limited slip and strain redistribution before failure. This mechanism reduces the initial stiffness but enhances the element's ability to absorb energy and undergo larger deformations prior to collapse, resulting in an overall improvement in ductility. That highlight the need for further study on whether controlled joint introduction can be applied as a seismic design strategy.

- The study's findings should be interpreted with caution due to several limitations. Scaled laboratory models differ from full-scale field behavior, especially in soil-structure interaction and boundary conditions. The use of polypropylene fibers instead of conventional reinforcement may reduce applicability to typical diaphragm walls. In addition, only static loading was examined, while real-world walls are often subjected to dynamic forces such as seismic activity and nearby construction. Therefore, field validation through case studies and monitoring of actual projects is essential to confirm the experimental results.

Acknowledgements

The authors would like to express their gratitude to the staff of the Structural Laboratory at University of Babylon.

Author Contributions

All authors critically reviewed and approved the final version of the manuscript and agreed to be accountable for all aspects of the work. All authors have accepted responsibility for the entire content of this manuscript and approved its submission.

Disclosure of Interest

The authors state no conflict of interest or personal relationships that could have appeared to influence the work reported in this paper.

Data Availability Statement

The data supporting the findings of this study are available from the corresponding author upon reasonable request.

Included in Article:

All data generated or analysed during this study are included in this published article.

References

A 615/A 615M - 15a. (2015). *Standard Specification for Deformed and Plain Carbon Steel Bars for Concrete*. American Society for Testing and Materials.

Addenbrooke, T. I. (1994). A flexibility number for the displacement controlled design of multi propped retaining walls. *Ground Engrg., London*, *September*, 41–45.

Al-Rubaye, M. M., Yousef, R. F., Muteb, H. H., & Al-Rubaye, M. M. (2020). Experimental evaluation of bond strength performance between normal concrete substrate and different overlay materials. *Journal of Engineering Science and Technology*, *15*(6), 4367–4382.

ASTM C469. (2011). Standard Test Method for Splitting Tensile Strength of Cylindrical Concrete Specimens. In *American Society for Testing and Materials (ASTM) International* (pp. 1–5). https://doi.org/doi: 10.1520/C0496.

ASTM C78/C78M-22. (2010). Standard test method for flexural strength of concrete (using simple beam with third-point loading). *American Society for Testing and Materials*, *100*, 12959–19428.

ASTM Standard C496. (2011). *Standard test method for splitting tensile strength of cylindrical concrete specimens*. ASTM international.

Barka, M., Taleb, O., Tedjditi, A. K., Soualhi, H., Benosman, A. S., & Mouli, M. (2024). Impact of polypropylene fibers on the rheological, mechanical, and thermal properties of self-compacting concrete. *MRS Advances*, *9*(14), 1128–1136. https://doi.org/10.1557/s43580-024-00905-1

Bleyhl, A. (2018). *Experimental Study on a New Type of Transverse Connection for Nebraska County Bridge System*.

BS EN 12390-3. (2009). Testing hardened concrete. Compressive strength of test specimens. *British Standards Institution, UK*.

Clough, G. W., and O'Rourke, T. D. (1990). Construction induced movements of insitu walls. In *Specialty Conference on Design and Performance of Earth Retaining Structures* (pp. 439–470). https://doi.org/10.1061/(ASCE)0733-9410(1992)118:4(662.2)

Comodromos, E. M., Papadopoulou, M. C., & Konstantinidis, G. K. (2013). Effects from diaphragm wall installation to surrounding soil and adjacent buildings. *Computers and Geotechnics*, *53*, 106–121. https://doi.org/10.1016/j.compgeo.2013.05.003

de Alencar Monteiro, V. M., Lima, L. R., & de Andrade Silva, F. (2018). On the mechanical behavior of polypropylene, steel and hybrid fiber reinforced self-consolidating concrete. *Construction and Building Materials*, *188*, 280–291. https://doi.org/https://doi.org/10.1016/j.conbuildmat.2018.08.103

Deng, H.-S., Fu, H.-L., Yimin, wu, Zhao, Y.-B., & Yi, H.-D. (2023). Fatigue fracture experiment of concrete members with cold joints under low stress and low stress amplitude fatigue load. *Theoretical and Applied Fracture Mechanics*, *127*, 104041. https://doi.org/10.1016/j.tafmec.2023.104041

EFNARC. (2005). *The European Guidelines for Self-Compacting Concrete,Specification and Production and Use*. Association House, UK.

Feng, P., Cheng, S., Bai, Y., & Ye, L. (2015). Mechanical behavior of concrete-filled square steel tube with FRP-confined concrete core subjected to axial compression. *Composite Structures*, *123*. https://doi.org/10.1016/j.compstruct.2014.12.053

Feng, P., Qiang, H., & Ye, L.-P. (2017). Discussion and definition on yield points of materials, members and structures. *Gongcheng Lixue/Engineering Mechanics*, *34*, 36–46. https://doi.org/10.6052/j.issn.1000-4750.2016.03.0192

Gaba, A. R., Simpson, B., Beadman, D. R., & Powrie, W. (2003). Embedded retaining walls: Guidance for economic design. *Proceedings of the Institution of Civil Engineers: Geotechnical Engineering*, *156*(1), 13–15. https://doi.org/10.1680/geng.2003.156.1.13

Houhou, M. N., Emeriault, F., & Belounar, A. (2019). Three-dimensional numerical back-analysis of a monitored deep excavation retained by strutted diaphragm walls. *Tunnelling and Underground Space Technology*, *83*, 153–164.

Iraqi Specification No.5. (2019). *Cement Portland* (pp. 21–23). National Center for Structural Laboratory, Planning Council, Baghdad, Iraq.

Iraqi specification requirements IQ.S 45. (2016). *Aggregates of Natural Resources used for Concrete and Construction*. National Center for Structural Laboratory, Planning Council, Baghdad, Iraq.

John Newman, B. S. C. (2003). *Advanced_Concrete_Technology_3_Processes.pdf*. Amsterdam : Elsevier, 2003.

Kisan, M., Sangathan, S., & Nehru, J. (1996). Design And Construction of Diaphragms for Under-Seepage Control - Code of Practice. In *Indian Standard*.

Li, K., Chen, S., Pei, R., & Li, Y. (2024). Theoretical Study on Diaphragm Wall and Surface Deformation Due to Foundation Excavation Based on Three-Parameter Kerr Model. In *Sustainability (Switzerland)* (Vol. 16, Issue 6). https://doi.org/10.3390/su16062295

Lim, A., Ou, C.-Y., & Hsieh, P.-G. (2018). Investigation of the integrated retaining system to limit deformations induced by deep excavation. *Acta Geotechnica*, *13*. https://doi.org/10.1007/s11440-017-0613-6

Liu, Y., Yang, G., Qi, C., Zhang, P., Cui, T., & Song, R. (2025). Experimental and Numerical Research on the Mechanical Properties of a Novel Prefabricated Diaphragm Wall–Beam Joint. *Buildings*, *15*(7), 1–19. https://doi.org/10.3390/buildings15071158

Mana, A. I., and C. (1981). Prediction of movements for braced cuts in clay. *Journal of Geotechnical and Geoenvironmental Engineering*, *107*(6), 759–777. https://doi.org/http://ojps.aip.org/gto

Mana, A. I., & Clough, G. W. (1981). PREDICTION OF MOVEMENTS FOR BRACED CUTS IN CLAY. *Journal of the Geotechnical Engineering Division*, *107*(6), 759–777. https://doi.org/10.1061/ajgeb6.0001150

Mhawish, A. H., & Risan, H. K. (2024). The Behavior of Concrete Cantilever Retaining Walls During Far-Field and Near-Fault Earthquakes. *Civil and Environmental Engineering*, *20*(1), 14–26. https://doi.org/10.2478/cee-2024-0002

Mohod, M. V. (2015). Performance of polypropylene fibre reinforced concrete. *IOSR Journal of Mechanical and Civil Engineering*, *12*(1), 28–36.

Moormann, C. (2004). Analysis of wall and ground movement due to deep exavation in soft soil based on a new worldwide data ase. *Soil and Foundation*, *44*(1), 87–98.

Ouedraogo, I., Ouadif, L., & Bahi, A. (2025). Diaphragm Wall Behaviour Under Thick Alluvium Layer Conditions. *Civil and Environmental Engineering*, *21*(1), 51–64. https://doi.org/10.2478/cee-2025-0005

Park, R., & Paulay, T. (1991). *Reinforced concrete structures*. John Wiley & Sons.

Pereira, J. R., Palma E Silva, J. B. L., Gachet, L. A., Dos Santos, A. C., & Lintz, R. C. C. (2023). Evaluation of the Addition of Polypropylene (PP) Fibers in Self-compacting Concrete (SCC) to Control Cracking and Plastic Shrinkage between Different Methods. In *Materials Research* (Vol. 26). https://doi.org/10.1590/1980-5373-MR-2022-0567

Potts, D. M., and Day, R. A. (1990). Discussion. Use of Sheet Pile Retaining Walls for Deep Excavations in Stiff Clay. *Proceedings of the Institution of Civil Engineers, London, Part 1*, *88*, 899–927. https://doi.org/10.1680/iicep.1991.17394

Qiu, T., Zhang, J., Chen, X., Xu, Z., Su, D., Song, R., & Cui, T. (2023). Experimental investigation and mechanical model for assembled joints of prefabricated two-wall-in-one diaphragm walls. *Engineering Structures*, *275*, 115285.

Reddy, T., & Reddy, D. (2023). Destructive and Non-Destructive Analysis of Polypropylene Fibre Reinforced Concrete. *International Journal of Scientific Research in Science and Technology*, 79–88. https://doi.org/10.32628/IJSRST52310313

Roesler, J. (2019). Effect of Macrofibers on Behavior and Performance of Concrete Slabs and Overlays. In *National Concrete Consortium*.

Sika's ViscoCrete 180G. (2022). *https://irq.sika.com/en/construction/concrete-admixtures/sika-viscocrete-180g.html* (p. Version 04.02).

Spruit, R., van Tol, F., Broere, W., Doornenbal, P., & Hopman, V. (2017). Distributed temperature sensing applied during diaphragm wall construction. *Canadian Geotechnical Journal*, *54*(2), 219–233.

Spruit, R., van Tol, F., Broere, W., Slob, E., & Niederleithinger, E. (2014). Detection of anomalies in diaphragm walls with crosshole sonic logging. *Canadian Geotechnical Journal*, *51*(4), 369–380.

Superczyńska, M., Józefiak, K., & Zbiciak, A. (2016). Numerical Analysis of Diaphragm Wall Model Executed in Poznań Clay Formation Applying Selected FEM Codes. *Archives of Civil Engineering*, *62*, 207–224. https://doi.org/10.1515/ace-2015-0093

Wang, J., Xiong, W., & Cai, C. S. (2024). Flexural performance of rigid joints for diaphragm walls: Experimental investigation and numerical analysis. *Case Studies in Construction Materials*, *20*, e02936. https://doi.org/https://doi.org/10.1016/j.cscm.2024.e02936

Yan, N., Li, G., Qin, F., Qiao, X., Lu, B., Liang, N., & Zhao, S. (2025). Study on the deformation characteristics of diaphragm walls in deep excavations within the Ningbo soft soil region. *Scientific Reports*, *15*(1), 15036.

https://doi.org/doi.org/10.1038/s41598-025-95878-y

Yang, M., Wu, R., Tong, C., Chen, J., & Tang, B. (2024). Displacement Analyses of Diaphragm Wall in Small-Scale Deep Excavation Considering Joints between Panels. In *Buildings* (Vol. 14, Issue 5). https://doi.org/10.3390/buildings14051449

Yousef, R. F., Al-Rubaye, M. M., & Muteb, H. H. (2022). Mechanical and chemical bond for composite action of precast beams. In *Curved and Layered Structures* (Vol. 9, Issue 1, pp. 304–319). https://doi.org/10.1515/cls-2022-0024

Yousef, R. F., Muteb, H. H., & Ibrahim, A. A. (2023). Studying the effect of embedded length strength of concrete and diameter of anchor on shear performance between old and new concrete. In *Curved and Layered Structures* (Vol. 10, Issue 1). https://doi.org/10.1515/cls-2022-0184

Zhang, W., Hong, L., Li, Y., Zhang, R., Goh, A. T. C., & Liu, H. (2021). Effects of jet grouting slabs on responses for deep braced excavations. *Underground Space*, *6*(2), 185–194. https://doi.org/https://doi.org/10.1016/j.undsp.2020.02.002

How to Cite This Article

Yousef, F. R., Muteb, H.H., & Al-Janabi, A. (2026). Experimental Investigation of Wall Thickness Effect on Cold Joints in a Scaled Diaphragm Wall Model Using Fiber-Reinforced Self-Compacting Concrete. Civil and Environmental Engineering, 0 (0). https://doi.org/10.2478/cee-2026-0067